



**Independent Off Site Evaluation of Electrical Power Generation by
BlackLight Power's High-Power-Density Catalyst Induced Hydrino
Transition (CIHT) Cells**

**Confidential Report Submitted
to**

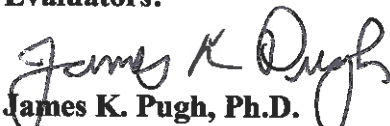
BlackLight Power, Inc
493 Old Trenton Road, Cranbury, NJ 08512

By

The ENSER Corporation
5430 70th Ave North, Pinellas Park, FL 33781

Dated 16th January 2013

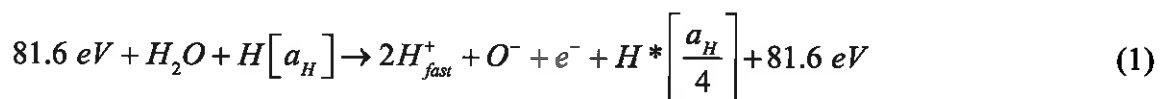
Evaluators:


James K. Pugh, Ph.D.
Director of Technology


Ethirajulu Dayalan, Ph.D.
Technical Fellow

Background

Dr. Randell Mills of BlackLight Power, Inc. (BLP) has developed the “Grand Unified Theory of Classical Physics,” by the application of physical laws and first principles rather than pure mathematics¹. Based on this theory, Dr Mills has calculated, with great precision, bond energies and molecular structures that have been verified through experimental observation and reported in the literature. Classical physical laws predict that there is a more stable lower energy state of hydrogen than previously believed. Specifically, atomic hydrogen may undergo a catalytic reaction with certain species, including itself, that can accept energy in integer multiples of the potential energy of atomic hydrogen, $m \cdot 27.2$ eV, wherein m is an integer. The predicted reaction involves a resonant, nonradiative energy transfer from otherwise stable atomic hydrogen to the catalyst capable of accepting the energy. The product is $H(1/p)$, fractional Rydberg states of atomic hydrogen called “hydrino atoms,” wherein $n = 1/2, 1/3, 1/4, \dots, 1/p$ ($p \leq 137$ is an integer) replaces the well-known parameter $n = \text{integer}$ in the Rydberg equation for hydrogen excited states. Each hydrino state also comprises an electron, a proton, and a photon, but the field contribution from the photon increases the binding rather than decreasing it corresponding to energy desorption rather than absorption. A molecule that accepts $m \cdot 27.2$ eV from atomic H with a decrease in the magnitude of the potential energy of the molecule by the same energy may serve as a catalyst. The potential energy of H₂O is 81.6 eV [1]; so, the nascent H₂O molecule (not hydrogen bonded in solid, liquid, or gaseous state) may serve as a catalyst. Based on the 10% energy change in the heat of vaporization in going from ice at 0°C to water at 100°C, the average number of H bonds per water molecule in boiling water is 3.6 [1]; thus, H₂O must be formed chemically as isolated molecules with suitable activation energy in order to serve as a catalyst to form hydrinos. The catalysis reaction ($m=3$) regarding the potential energy of nascent H₂O is



And, the overall reaction is



¹ R. Mills, *The Grand Unified Theory of Classical Physics*, July 2010 edition, <http://www.blacklightpower.com/theory/bookdownload.shtml>.

BLP has invented an electrochemical cell, a hydrino fuel cell called a CIHT (**Catalyst-Induced-Hydrino-Transition**) cell that generates an electromotive force (EMF) from the catalytic reaction of hydrogen to lower energy (hydrino) states providing direct conversion of the energy released from the hydrino reaction into electricity. Each CIHT cell shown schematically in Figure 1 contains a cathode, an anode, and an electrolyte that also serves as a source of reactants to form hydrinos. Due to oxidation-reduction half cell reactions, a hydrino-producing reaction mixture is constituted with the migration of electrons through an external circuit and ion mass transport through a separate internal path through the electrolyte to complete an electrical circuit. In one type of electrolytic regenerative CIHT cell, atomic hydrogen and oxygen are intermittently formed by electrolysis of H_2O in the cell. During cell discharge the nascent H_2O molecule formed by an oxidation reaction of OH^- and reaction with H at a hydrogen anode serves as a catalyst to form $H(1/4)$ with an energy release of 204 eV compared to the 1.48 eV required to produce H from the electrolysis of H_2O with a net gain of electrical output. A transition from hydrogen in the traditional molecular state, H_2 , to the hydrino state releases energy up to two hundred times greater than combusting the same amount of hydrogen, the fuel being only H_2O supplied to the electrolysis.

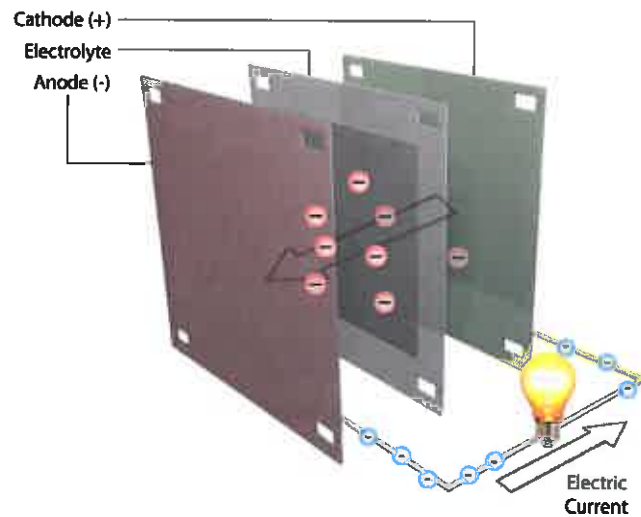


Figure 1. Schematic of CIHT Cell.

On Site Validation of CIHT Cells by ENSER

As discussed in the validation study report from ENSER dated April 4, 2012, ENSER technical staff witnessed on February 12, 2012 careful assembly of four closed CIHT cells supplied with H₂O vapor entrained in an inert (argon) carrier gas as the only mass input. The cells were run under intermittent electrolysis condition to generate hydrogen at the anode and oxygen at the cathode. Three of the test cells were comprised of pre-oxidized porous nickel cathode, LiOH-LiBr-MgO electrolyte, and pressed porous nickel anode. A fourth test cell used a molybdenum (Mo) anode. The startup of the cells and data collection setup was also witnessed. Initial data indicated that all four cells showed excess energy production during discharge compared to the energy input during short charge pulses. The Mo anode cell showed much higher energy discharge excess than the nickel anode cells. Periodic updates of the data from the cells built for ENSER validation were sent by BLP staff. The cells ran for nearly forty days before they were stopped with ENSER's concurrence. The cells with nickel anodes showed an energy gain of 332%, 8625% and 793% in 39 days and the cell with the Mo anode showed 144028% energy gain in about 39 days.

Control cells were also built during the visit where the electrolyte was different than the optimized CIHT cell electrolyte or where the cell is run without the supply of water vapor wherein the chemically similar, but not hydrino catalytic cells showed an energy loss and the otherwise active chemistry lacking the required H₂O quickly decayed to zero power.

No readily recognized reaction is expected to occur at the electrodes or the electrolyte that could produce the observed electrical energy. Furthermore, there is no possible reaction of H₂O with the cell constituents based on system thermodynamics. Dr. Mills' theory offers a plausible explanation: H formed during electrolysis undergoes a reaction to form hydrinos with the release of electrical energy. Results were consistent with the proposed CIHT cell half-cell reactions forming the hydrino catalyst in the presence of atomic hydrogen, and the cell performance matched predictions based on the hydrino mechanism including the upfield NMR results characteristic of the hydrino product. Albeit these first generation CIHT cells served as a proof of principle of the breakthrough new source of electricity, the power density was low, about 0.2 mW/cm² and correspondingly, the cell power was low, about 2-3 mW.

Off Site Independent Evaluation of CIHT Cells by ENSER

ENSER has undertaken off site independent evaluation study of BLP's improved high power CIHT cells. Dr. James Pugh (Electrolyte Scientist and Director of Technology at The ENSER Corporation) and Dr. Ethirajulu Dayalan (Electrochemist and Technical Fellow at The ENSER Corporation) conducted independent tests of CIHT cells at ENSER's facility at Pinellas Park, FL between August and December, 2012. The main purpose was to independently validate BlackLight's results off site by an unrelated highly qualified third party. The second purpose was to determine if hydrino was the product of any excess electricity observed. The third purpose was to determine whether BlackLight Power had achieved high power density with stabilization of the anode from corrosion by maintaining a negative operating voltage relative to the thermodynamic anode corrosion voltage and by the presence of hydrogen supplied to the anode through the hydrogen permeable membrane.

Representatives from Prokon Energy (Germany) visited ENSER during this period and witnessed the experimental set up, assembly of the cells, testing and data collection at ENSER. Figure 1 shows the representatives next to some of the CIHT and control cells at ENSER. Another independent consultant who evaluated BLP's CIHT cell technology also visited ENSER during this period and witnessed the cell assembly and test runs.



Figure 2. Prokon Representatives Witnessing CIHT Cells at ENSER.

ENSER – BlackLight Power Confidential Communication

The CIHT cells in this study comprising the catalytic anode, cathode and electrolyte combination were tested for hydrino formation as a half-cell reaction to serve as a new electrical energy source wherein the power density was increased by a factor of up to 50 times than that of the prior CIHT cells.

Nearly 30 tests were conducted at ENSER. The tests fall into two categories. One set consisted of CIHT Cells where the anode, cathode and electrolyte combinations that produced catalytic effect and excess energy and are listed in Table I. The second set consisted of anode, cathode and electrolyte combination that did not generate excess energy. The discharge energy in this set of cells is less than the charge energy or sometimes negligible. The second set is referred to as Control Cells and is listed in Table II.

Table I: CHIT Cells Tested at ENSER

Blacklight Power CIHT Cells - Validation Runs at ENSER

test #	START DATE	Run Time Hours	Charge Energy	Discharge Energy (Wh)	Energy Gain %	Anode atomic %	Electrolyte	Cell Type
1	9/25/2012	48.00	1.22	2.17	78.1	50:50 Mo:Ni	LiOH+LiBr	Open Air
2	9/28/2012	48.00	0.88	1.59	79.6	Mo	LiOH+LiBr	Open Air
3	9/28/2012	48.00	1.16	1.87	61.2	Mo	LiOH+LiBr	Open Air
4	10/4/2012	48.00	1.29	2.36	83.4	50:50 Mo:Ni	LiOH+LiBr	Closed Cell - Getter
5	10/4/2012	48.00	0.78	1.48	89.3	50:50 Mo:Cu	LiOH+LiBr	Open Air-H2 PERM
6	10/11/2012	48.00	0.78	1.48	90.3	50:50 Mo:Cu	LiOH+LiBr	Open Air-H2 PERM
7	10/18/2012	48.00	0.76	1.45	90.0	Mo	LiOH+LiBr	Open Air-H2 PERM
8	10/23/2012	48.00	0.78	1.49	91.5	Mo	LiOH+LiBr	Open Air-H2 PERM
9	10/23/2012	48.00	0.35	0.65	86.9	50:50 Mo:Cu	LiOH+LiBr	Open Air
10	10/23/2012	48.00	0.89	1.56	75.3	Mo	LiOH+LiBr	Open Air
11	11/15/2012	48.00	0.81	1.49	83.9	Tapecast 90:10 Ni:Co (wt %)	LiOH+LiBr	Open Air
12	11/27/2012	42.71	0.72	1.34	86.2	50:50 Mo:Cu	LiOH+LiBr	Open Air-H2 PERM
13	11/28/2012	48.00	0.85	1.52	78.7	Mo	LiOH+LiBr	Closed Cell - Getter
14	12/12/2012	48.00	0.85	1.62	90.4	Tapecast 82:18 Co:Cu (wt %)	LiOH+LiBr	Open Air-H2 PERM

Table II: Control Cells Tested at ENSER

Blacklight Power Control Cells - Validation Runs at ENSER

test #	START DATE	Run Time Hours	Charge Energy	Discharge Energy (Wh)	Energy Gain %	Anode atomic %	Electrolyte	Cell Type
1	8/13/2012	26.37	1.52	1.10	-27.9	50:50 Mo:Cr	LiOH+LiBr	Open Air
2	8/13/2012	134.91	8.68	5.88	-32.2	80:20 Mo:Cr	LiOH+LiBr	Open Air
3	8/15/2012	82.53	4.47	3.30	-26.2	50:50 Mo:Cr	LiOH+LiBr	Open Air
4	9/6/2012	48.00	3.39	1.90	-43.8	80:20 Mo:Cr	LiOH+LiBr	Open Air
5	9/6/2012	23.89	2.01	0.82	-59.2	50:50 Mo:Cr	LiOH+LiBr	Open Air
6	9/25/2012	48.00	3.26	1.90	-41.8	50:50 Mo:Cr	LiOH+LiBr	Open Air
7	9/25/2012	48.00	1.72	1.41	-18.4	80:20 Mo:Cr	LiOH+LiBr	Open Air
8	10/23/2012	48.00	2.84	0.03	-99.0	Mo	KOH+KBr	Open Air-H2 PERM
9	11/6/2012	18.01	1.11	0.25	-77.1	Mo	KOH+KBr	Open Air
10	11/6/2012	44.76	0.82	0.00	-99.9	50:50 Mo:Cu	KOH+KBr	Open Air
11	11/9/2012	48.00	1.41	0.00	-100.0	50:50 Mo:Cu	KOH+KBr	Open Air-H2 PERM
12	11/15/2012	47.53	1.67	0.00	-99.8	Tapecast 90:10 Ni:Co (wt %)	KOH+KBr	Open Air
13	11/28/2012	9.31	0.67	0.06	-90.4	Mo	KOH+KBr	Open Air
14	11/27/2012	39.71	1.41	0.00	-99.9	50:50 Mo:Cu	KOH+KBr	Open Air-H2 PERM
15	12/3/2012	48.00	3.06	0.87	-71.5	Mo	KOH+KBr	Open Air

CIHT cells (Table I) are comprised of a LiOH-LiBr eutectic mixture as the electrolyte, NiO as the cathode and MoNi (50-50 at%), Mo, MoCu (50-50 at%), NiCo (90-10 wt%) or CoCu (82-18 wt%) as the anode.

Control cells (Table II) contain either a different electrolyte (typically KOH-KBr eutectic mixture) or a different anode compared to the CIHT Cells.

The cathode is always a cylindrical NiO cathode with a stainless steel lead wire and is shown in Figure 3. The anodes are in the shape of a circular pellet ($\sim 1\text{cm}^2$) or a 1cm x 1cm foil with nickel lead wires, or a hydrogen permeable membrane electrode made up of two welded 3.5 cm or 3.8 cm diameter discs and a Ni or SS tube attached for hydrogen supply which also serves as an electrical lead. The different anodes are shown in Figure 4. Figure 5 shows a typical electrode arrangement where the anode and cathode are mechanically separated using a ceramic ring and a ceramic tube. The cell container is a ceramic cylindrical crucible shown in Figure 6. The ceramic tube is placed inside a steel crucible housed inside an insulated furnace. Figure 7 shows several of the furnaces with operating cells at ENSER. An Arbin BT 2000 battery tester was used for charge discharge tests and for gathering data including the cumulative input and output energies with time. An oscilloscope was used to verify and capture the current voltage signals. Figure 8 shows this arrangement at ENSER.



Figure 3. Cylindrical NiO Cathode.

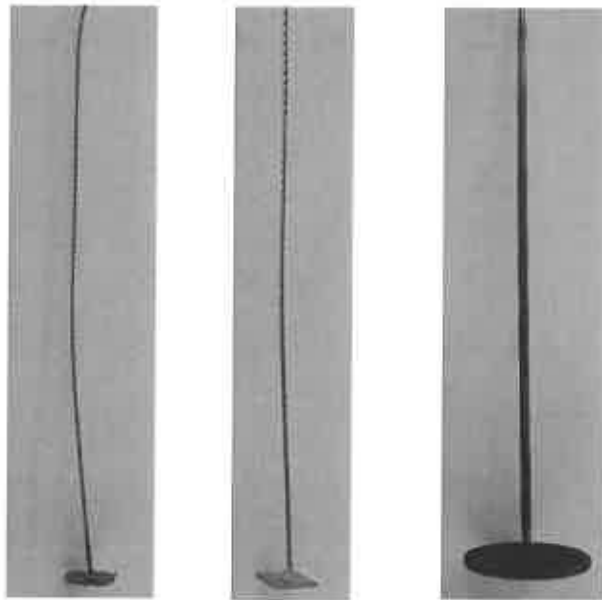


Figure 4. Different Types of Anodes Used in the Study. From Left to Right: Pellet, Foil and, Hydrogen Permeable Disc.

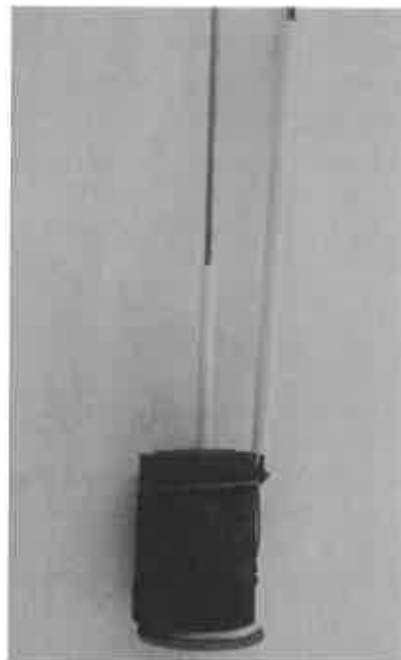


Figure 5. Electrode Arrangement with a Hydrogen Permeable Anode. Ceramic-Spacer Ring and Ceramic Tube Separate Anode and Cathode.



Figure 6. Ceramic Cylindrical Crucible Cell Container.



Figure 7. Four of the Test Cells in Operation at ENSER.

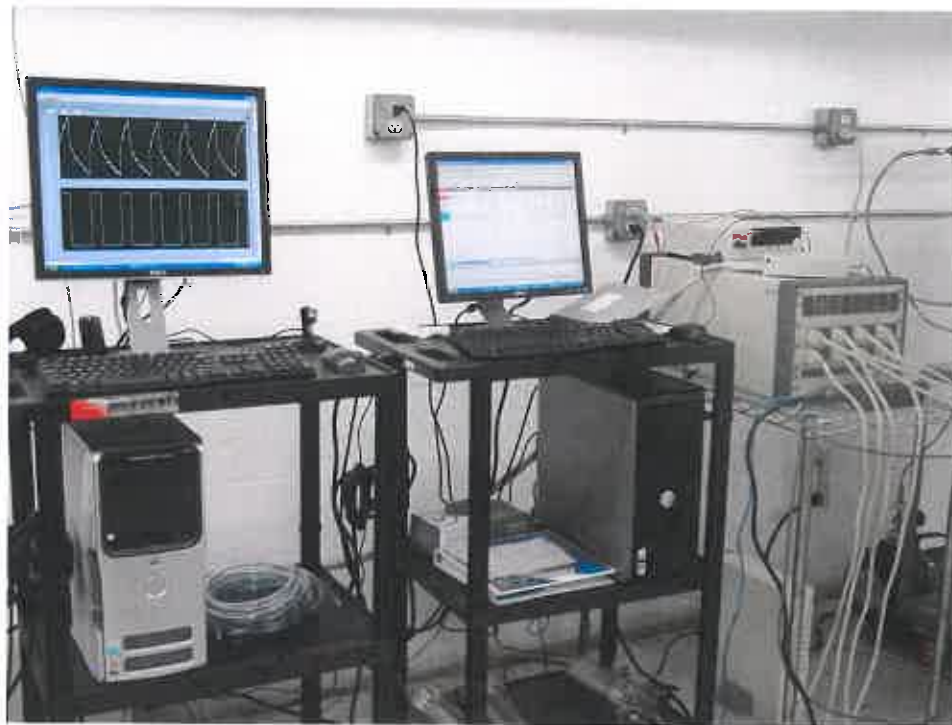


Figure 8. ARBIN BT 2000 Tester and Oscilloscope Arrangement.

For the electrochemical testing, the electrolyte was first heated in the ceramic crucible placed inside the furnace. After electrolyte melting and the temperature reaching a steady value of about 430°C the preassembled electrode arrangement was dipped into the molten electrolyte. The electrical connections are then made and the predetermined charge discharge test profile begun. The cells were operated under intermittent H_2O electrolysis to generate hydrogen at the anode and oxygen at the cathode then discharged to form hydrinos wherein H_2O vapor as well as some O_2 was supplied from the atmosphere in open cells. Net electrical production over the electrolysis input (and hydrogen supplied to the anode in cells with hydrogen permeation anodes) was measured using the Arbin BT 2000 ($<0.1\%$ error) and confirmed using the digital oscilloscope. A possible anode-air reaction was tested by measuring the thickness of the anodes before and after operation as well as by comparison to a control electrolyte that was capable of a greater rate of metal oxidation but did not produce excess electrical energy. Characteristic signatures of the hydrino products were sought using three analytical techniques.

An exemplary CIHT cell comprised of (i) a 6.5 cm ID X 14 cm IH alumina crucible containing the cell components and (ii) (a) Mo or MoCu (50-50 at%, AMETEK) hydrogen permeable anode comprising a diaphragm made of two pieces of 3.5 cm or 3.8 cm OD (1mm or 0.5mm thickness foils welded together and joined to a 0.95 cm or 0.625 cm OD Ni H_2 supply tube). The hydrogen

was supplied from a two liter tank having H₂ pressure in the range of 950±30 Torr monitored using a Baratron gauge; (b) Mo or MoCu (50-50 at%, AMETEK) foil anode, 1 cm X 1 cm; (c) MoNi (50-50 at%) pellet anode, 1 cm diameter, or (d) NiCo (90-10 wt%) tape cast anode 3.8 cm OD; (e) CoCu (82-18 wt%) tape cast anode 3.8 cm OD that was clad onto a 2.22 cm OD H₂ permeable 0.25 mm thick Ni membrane of the same construction as the Mo and MoCu membranes by 2 ton compression, (iii) a NiO cylindrical cathode, 3.8cm OD x 1cm ID x 5cm tall, pre-oxidized porous Ni C6NC (Sumitomo Electric oxidized in air at 800°C for 4 h) placed on top of the electrolyte, and (iv) a molten eutectic salt electrolyte comprising LiOH (15 g)-LiBr (75 g). The electrode spacing was 0.2-0.3 cm maintained by an alumina spacer ring. The alumina crucible containing the cell components was placed in a resistive heater that maintained the temperature of the electrolyte at 430 ±2 °C. The cell was operated open to atmosphere. Control cells of the anode metal-air reaction as a source of electricity comprised identical cells with the LiOH-LiBr electrolyte replaced by KOH (61.8 g) -KBr (51 g) that has a much higher oxygen reduction rate and is predicted to be a superior electrolyte for any possible metal-air contribution to the energy balance.

Nickel leads from the anode and stainless steel leads from the cathode were attached to the leads of the calibrated Arbin BT2000 fuel cell and battery testing system. The cell was run under intermittent electrolysis conditions. The programmed waveform typically comprised the steps of (i) charge at constant current such as 50 mA for 1s duration and (ii) discharge at 50 mA constant current for 2s duration. The Arbin BT2000 voltage and current waveforms were confirmed with the digital oscilloscope.

Analytical Samples for the Spectroscopic Identification of Molecular Hydrino: CIHT cells having a molten LiOH-LiBr electrolyte and Mo or MoCu alloy anodes served as sources of the theoretically predicted molecular hydrino product H₂(1/4). Magic angle spinning ¹H nuclear magnetic resonance spectroscopy (MAS ¹H NMR), Raman spectroscopy, and photoluminescence emission spectroscopy were performed on reaction products. The molecular hydrino samples were generated from CIHT electrodes and captured by the inorganic compound getters (KOH-KCl mixtures placed in a sealed container and included in closed CIHT cells). Water vapor was supplied by moist air wherein hydrinos generated during operation were trapped in the matrix of the compound that served as a molecular hydrino getter. Starting KOH-KCl mixture samples not exposed to a hydrino source served as controls.

MAS 1H NMR: 1H MAS NMR was performed on solid samples using a 270 MHz instrument with a spin speed of 4.5 kHz. Side bands were eliminated by spinning at two different speeds. Chemical shifts were referenced to external TMS.

Raman Spectroscopy: Raman spectroscopy was performed on solid samples using a Horiba Jobin Yvon LabRAM Aramis Raman spectrometer with a 325 nm HeCd laser that was operated in microscope mode with a magnification of 40X. Additionally, spectra were obtained on MoCu anodes rinsed with deionized H_2O using a Thermo Scientific DXR SmartRaman spectrometer having a 780 nm diode laser. The resolution, depending on the instrument focal length, wavelength range, and grating, was typically 1 - 5 cm^{-1} .

Results

CIHT Cell Electrical Energy Balances

A typical oscilloscope scan of voltage and current waveforms is shown Figure 9. The graphs in Figures 10 and 11 show typical plots of various parameters of a 48 hour net energy producing CIHT cell test and a control test where the net energy is negative, respectively. Table I and Table II list the energy gain in CIHT cell tests and the energy loss in Control cell tests.

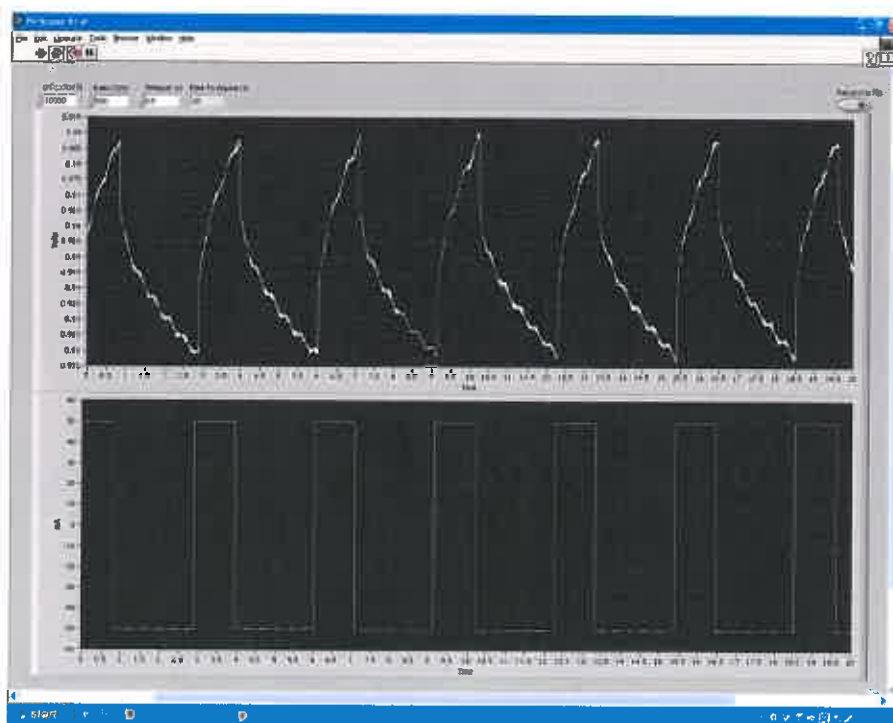


Figure 9. Oscilloscope Trace of the Charge – Discharge Waveform.

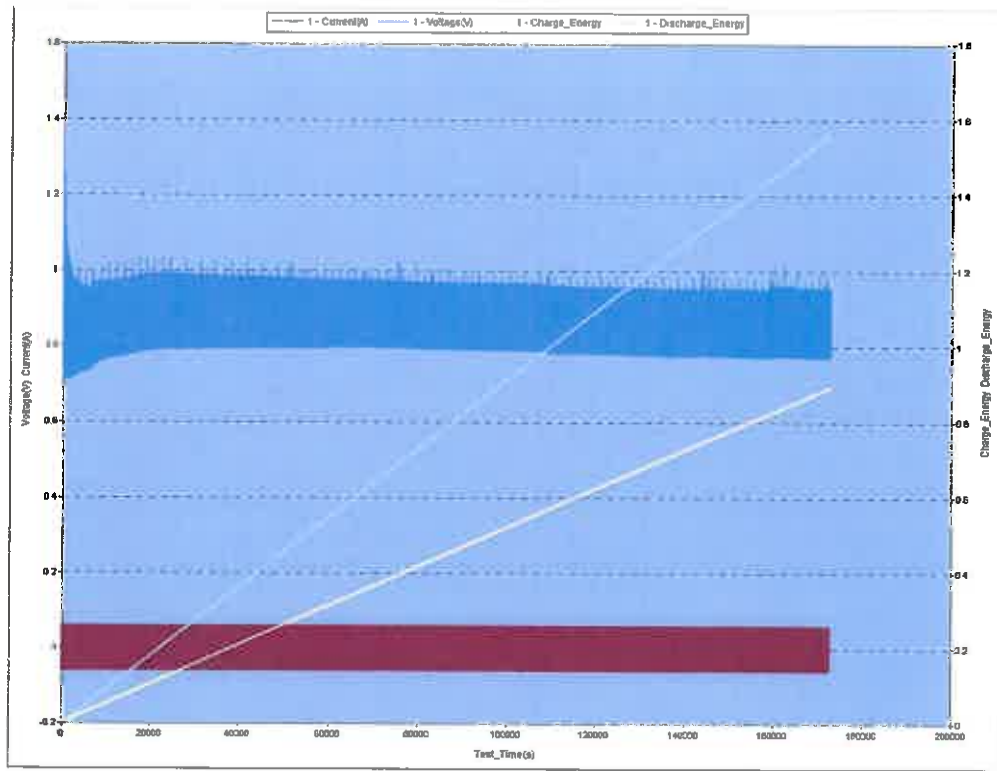


Figure 10. Plot of a Typical CIHT Cell Test – Net Positive Energy Producing Cell.

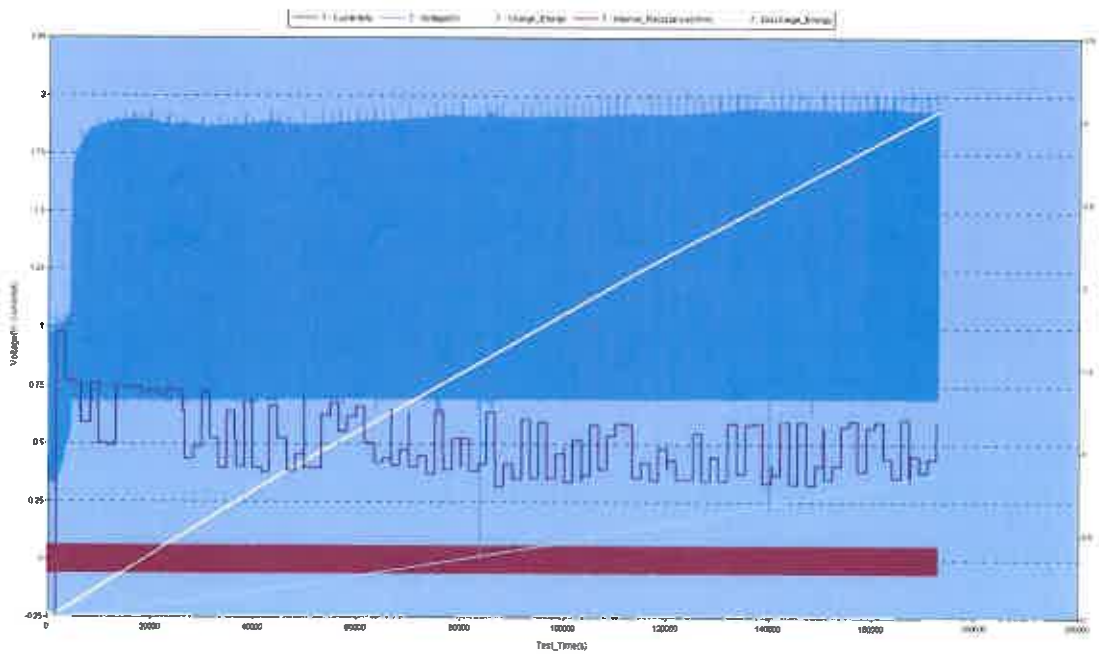


Figure 11. Plot of a Typical Control Cell Test – Net Negative Energy Producing Cell.

As shown in Table I, the electrical energies for CIHT cells comprising hydrogen permeable Mo or MoCu anodes and comprising foil membranes continuously output over 48 hour-duration were typically 1.8 times the electrical input at about 10 mW/cm² anode area. This is approximately a 50 times increase in power density compared to the cells of the ENSER April 2012 report. Using the maximum thermodynamic conversion of 200 kJ/mole H₂ to electricity, the contribution of the permeation hydrogen to the input power was low (<10% of the electrolysis contribution). Using a micrometer it was determined that there was no loss of metal from the hydrogen permeable membrane. The hydrogen protected the anode from corrosion whereas the metal foil anodes showed corrosion. Another benefit was that the cell voltage remained near the open circuit voltage and provided a reduction potential to further stabilize the anode.

The electrical energies continuously output over a 48 hour-duration for cells having foil anodes was also typically 1.8 times the electrical input at up to 100 mW/cm² anode area. Using a micrometer it was determined that there was loss of metal from the anode. Foil cells at BLP also showed metal loss even at much lower power densities. A hydrogen protective effect was clearly observed in the permeation anode cells.

Tape cast NiCo anodes were very stable in LiOH-LiBr electrolyte and developed about 4.5 mW/cm². This comprises approximately a 25-fold improvement over the crushed Ni celmet anodes of the ENSER April report. The CoCu tape cast-clad Ni permeable membrane showed a very slight weight gain likely due to residual electrolyte. There was no visible sign of corrosion demonstrating that H₂ protection can be applied to high surface area materials as well. Given that the surface area of tape cast material is orders of magnitude than that of foils, and the power density is very significantly improved with surface area, a similar factor of beyond the 500 fold increase with Mo or Mo-alloy foil may be anticipated.

The excess energy in either case cannot be attributed to a metal-air reaction as demonstrated by the results with the substitution of KOH-KBr for LiOH-LiBr. The energy balance was very low despite the metal corrosion being very high.

Spectroscopic Identification of Molecular Hydrino

BLP reported that the CIHT cell getter KOH-KCl showed a shift of the MAS NMR active component of the matrix (KOH) from +4.4 ppm to about -4 to -5 ppm after exposure to the atmosphere inside of the sealed CIHT cell. ENSER sent the samples to an independent lab for analysis and reproduced this result. For example, the MAS NMR spectrum of the initial KOH-KCl (1:1) getter and the same KOH-KCl (1:1) getter from a CIHT cells comprising [MoNi/LiOH-LiBr/NiO] that output about 2.5 Wh, 80 mA, at 180% gain (Figures 12 and 13) showed that the known downfield peak of the OH matrix shifted from about +4 ppm to the upfield region of about -4 ppm.

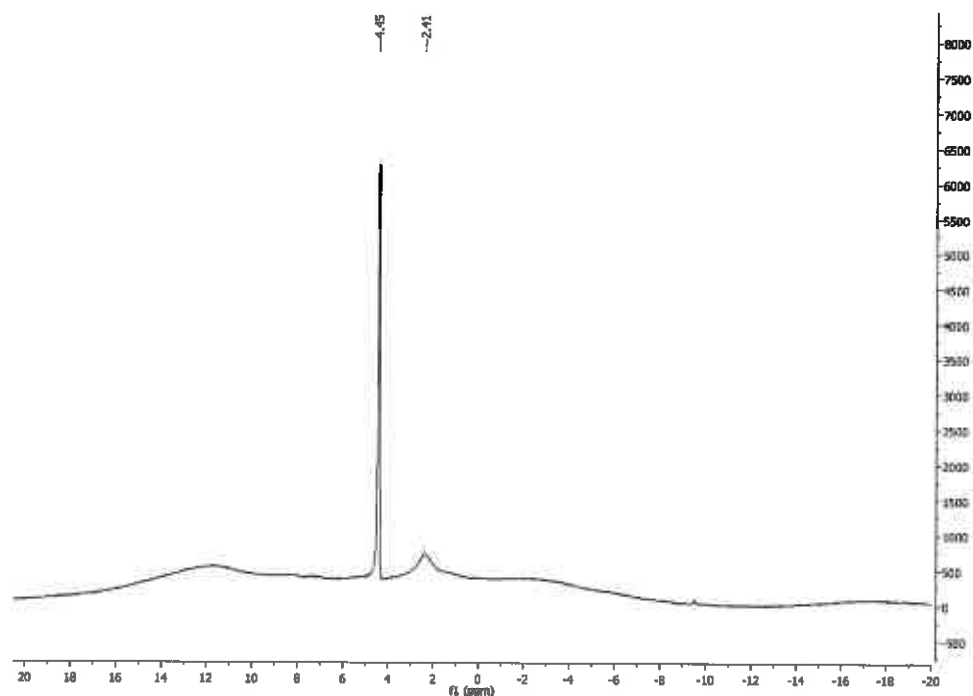


Figure 12. ^1H MAS NMR spectrum relative to external TMS of the initial KOH-KCl (1:1) getter that shows the known down-field shifted matrix peak at +4.45 ppm.

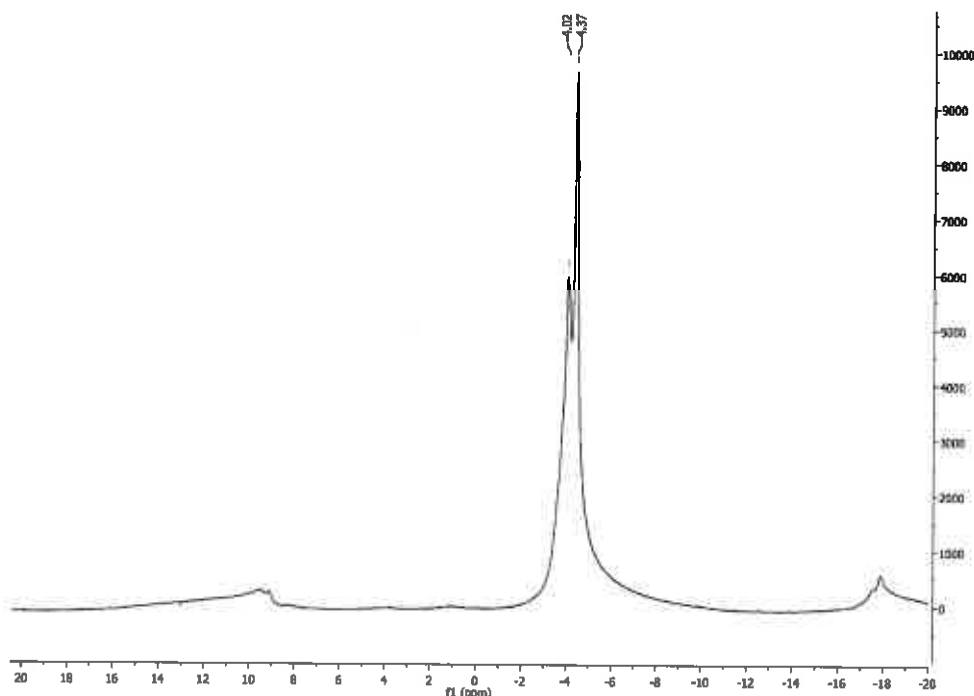
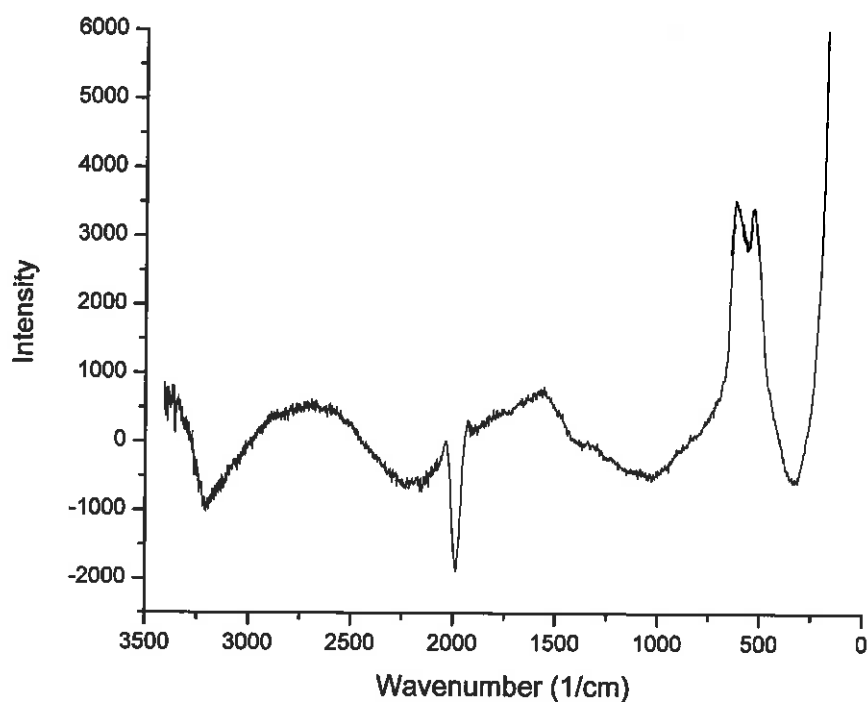
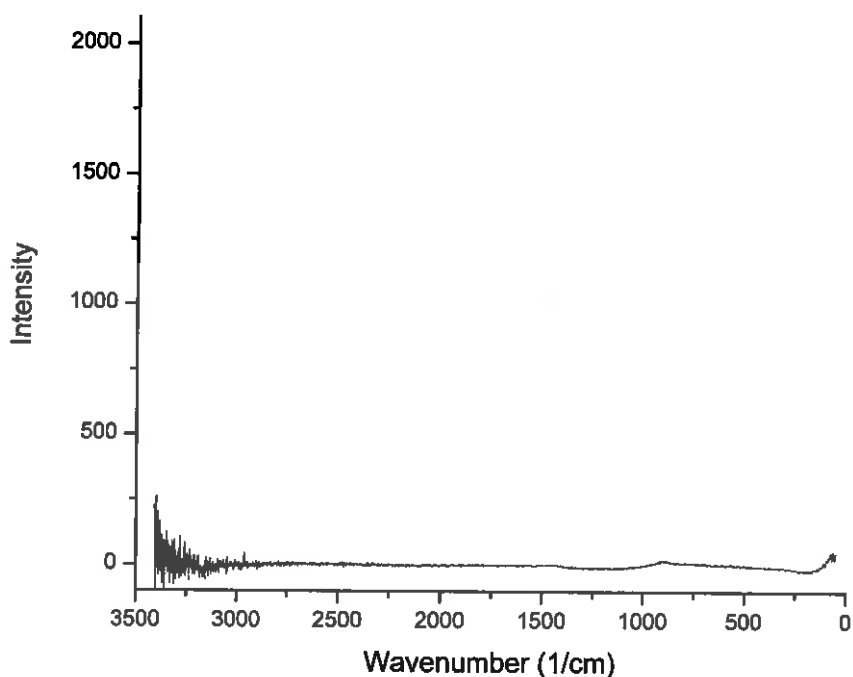


Figure 13. ^1H MAS NMR spectrum relative to external TMS of the KOH-KCl (1:1) getter from a CIHT cell comprising [MoNi/LiOH-LiBr/NiO] that output 2.36 Wh, 80 mA, at 183% gain that shows upfield shifted matrix peaks at -4.02 and -4.37 ppm. The symmetrically spaced peaks are spinning side bands.

Using a Thermo Scientific DXR SmartRaman with a 780 nm diode laser in the macro mode, a 40 cm^{-1} broad absorption peak was observed on MoCu hydrogen permeation anodes after the production of excess electricity (Figure 14). The peak was not observed in the virgin alloy (Figure 15), and the peak intensity increased with increasing laser intensity. The absorption peak starting at 1950 cm^{-1} (Figure 14) matched results from BLP that assign the peak to an inverse Raman effect from the free rotational energy of $\text{H}_2(1/4)$ (0.2414 eV , 1950 cm^{-1}) having a four significant figure match to theoretical predictions.



Figures 14. The Raman spectra obtained on MoCu anodes from CIHT cells comprising [MoCu/LiOH-LiBr/NiO] using a Thermo Scientific DXR SmartRaman spectrometer and a 780 nm laser showing a new sharp inverse Raman effect absorption peak starting at 1950 cm^{-1} that matches the free rotor energy of $\text{H}_2(1/4)$ (0.2414 eV) to four significant figures. The results are from a rinsed anode from the CIHT cell [MoCu (H permeation)/LiOH-LiBr/NiO] that output 1.48 Wh, 50 mA at 190% gain.



Figures 15. The Raman Spectra Obtained on MoCu Starting Material Showing no Peak at 1950 cm^{-1} .

Another successful confirmatory technique in the search for hydrino product spectra involved the use of the Raman spectrometer. The gas from a closed cell with the KOH-KCl (50-50 at%) getter [MoNi/LiOH/NiO] (2.36 Wh, 80 mA, 9.5V, at 183% gain) was used for Raman spectrum analysis using a Horiba Jobin Yvon LabRAM Aramis Raman spectrometer with a HeCd 325 nm laser in microscope mode with a magnification of 40X. In each case, an intense series of 1000 cm^{-1} (0.1234 eV) equal-energy spaced Raman peaks (Figure 16) were observed in the 8000 cm^{-1} to $18,000\text{ cm}^{-1}$ region. The conversion of the Raman spectrum into the fluorescence or photoluminescence spectrum revealed a match to BLP's reported spectra as the second order rovibrational spectrum of $\text{H}_2(1/4)^{2,3}$. The BLP peak assignments to the Q, R, and P branches for the spectra shown in Figure 15 are R(0), R(1), R(2), R(3), R(4), Q(0), P(1), P(2), P(3), P(4), P(5), and P(6) observed at 12,199, 11,207, 10,191, 9141, 8100, 13,183, 14,168, 15,121, 16,064, 16,993, and $17,892\text{ cm}^{-1}$, respectively.

² R. Mills J. Lotoski, J. Kong, G Chu, J. He, J. Trevey, "High-Power-Density Catalyst Induced Hydrino Transition (CIHT) Electrochemical Cell" (2012).

³ R. Mills, X Yu, Y. Lu, G Chu, J. He, J. Lotoski, "Catalyst induced hydrino transition (CIHT) electrochemical cell," (2012) submitted.

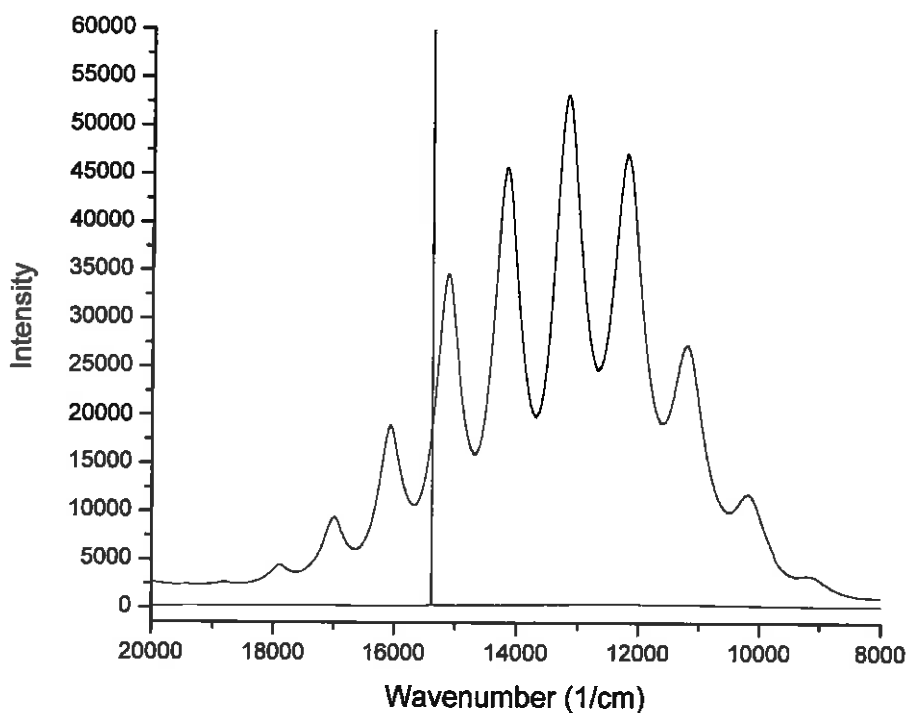


Figure 16. Raman-mode second-order photoluminescence (PL) spectra of the KOH-KCl (1:1) getter. Bottom trace: Initial KOH-KCl (1:1) getter. Top trace: PL band after exposure to gas from the CIHT cell comprising [MoNi/LiOH-LiBr/NiO] that output 2.36 Wh, 80 mA, at 183% gain.

Practical Considerations

The test cells that were assembled lend themselves with modifications to fabrication utilizing more traditional molten salt battery techniques (i.e. thermal batteries). The electrolyte salt composition is comprised of powdered materials and with binder immobilization and may be able to be pressed into pellet form utilizing the same high-tonnage pressing techniques that are employed in the thermal battery industry. The anodes and cathodes need modification for large-scale production, but there is no apparent difficulty in assembling single cell and multi-cell batteries, based on the electrochemistry discussed herein, in a production scale environment. CIHT cell Mo-based anodes can support $>100 \text{ mW/cm}^2$ power density from the hydride reaction without considering the improvement in power density from using high surface area materials versus foil. Since the power contribution from the permeation hydrogen that is capable of protecting the anode is only on the order of a few mW/cm^2 , 100 mW/cm^2 excess electricity over permeation is predicted while maintaining anode stability.

Moreover, engineering projections confirmed that a stack not requiring gas or heat handling systems is feasible wherein a 20 micron, porous cathode can support 100 mA/cm² from the hydrino reaction with 25 cm diameter plates. Considering the range of surface power densities with dimensions of 10 microns, 10 microns, and 20 microns for the anode, electrolyte layer and porous cathode, respectively, to provide H₂O transport to the reaction, volumetric power densities of 2.5 and 25 kW/liter are feasible with a corresponding material cost of about \$70 and \$7/kW, respectively.

Conclusion

ENSER has independently fabricated and tested CIHT cells successfully at their facility. The CIHT cells continuously produced net electrical energy output of approximately two times that of the input to maintain the process. The power generation is consistent with Dr. Mills theory of energy release resulting from hydrino formation. The power generation is not observed and is actually negative with control cells where a different electrolyte or anode is used. The predicted molecular hydrino H₂(1/4) was identified as a product of CIHT cells by MAS ¹H NMR, Raman spectroscopy, and photoluminescence emission spectroscopy.

The hydrogen permeation successfully stabilized the anode at power densities permissive of multi-kilowatts per liter in a final CIHT cell product. An improvement of at least 10 times this power density appears feasible which may reduce the cost of materials to under \$10/kW.

Representatives from another company and an independent consultant have witnessed the assembly of the cells and data collection at ENSER.